Catalysis Letters (2024) 154:3212–3224
https://doi.org/10.1007/s10562-023-04540-7

Hydrogenation of Cinnamaldehyde Using Carbon Dots Reduced Palladium Nanoparticles

Alice Magubane[1,2,3] · Prakash M. Gangatharan[1,2] · Pumza Mente[1,2] · Tumelo N. Phaahlamohlaka[2] · Manoko S. Maubane-Nkadimeng[1,2,4] · Michael Lee[5] · Jacques O'Connell[5] · Neil J. Coville[1,2]

Received: 14 August 2023 / Accepted: 24 November 2023 / Published online: 10 January 2024

Abstract

Carbon dots (CDs) with a size range of 0.2 to 2 nm were prepared using a hydrothermal treatment of sucrose and oleic acid. The as-synthesized CDs were used to reduce H_2PdCl_4 to metallic Pd nanoparticles with $d_{Pd} = 9.3 \pm 3.7$ nm, as confirmed by PXRD and HRTEM data. Pd particles were made to be larger than the CDs, to observe any inverse support effects, however, TEM data revealed that the CDs were transformed to carbon sheets in the reduction reaction at 100 °C. The synthesized Pd-CDs catalysts (0.81 wt. % loading) and CDs were both tested for the liquid phase hydrogenation of cinnamaldehyde. The influence of mass, temperature, and hydrogen flow rate on the activity and selectivity of the CDs and Pd-CDs catalyst on the hydrogenation of cinnamaldehyde was investigated. The CDs gave a cinnamaldehyde conversion (40%, 4 h) with selectivity towards the reduction of the C = O bond (cinnamyl alcohol) while the Pd-carbon catalyst was only selective to the reduction of the C = C bond (conversion 78%) indicating the dominance of Pd in the reaction. Post analysis of the deactivated catalysts indicated formation of carbon sheets and sintering of the Pd nanoparticles. It is thus shown that the presence of Pd induces the CDs to carbon sheet formation and thus indicates the limited use of CDs as a support for the olefin hydrogenation reaction with the CDs produced carbon support. This finding has implications for other studies using CDs as supports.

Graphical abstract

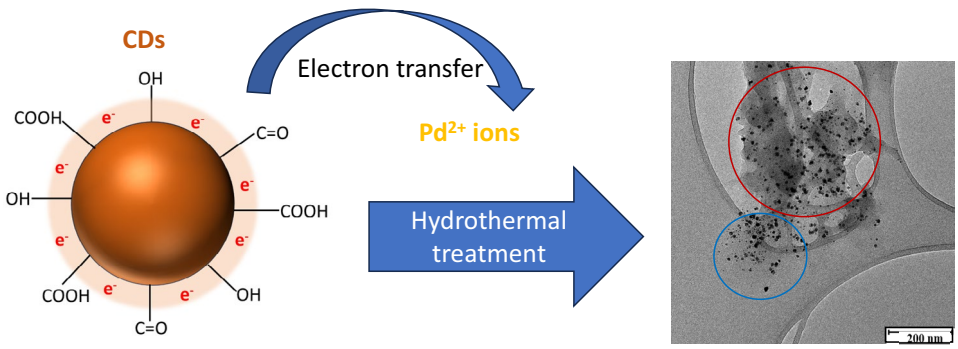

Keywords Carbon dots · Carbon sheets · Hydrogenation · Palladium · Cinnamaldehyde

✉ Neil J. Coville
neil.coville@wits.ac.za

[1] DSI-NRF Centre of Excellence in Strong Materials, University of the Witwatersrand, Johannesburg 2050, South Africa

[2] Molecular Sciences Institute, School of Chemistry, University of the Witwatersrand, Johannesburg 2050, South Africa

[3] Institute for Catalysis and Energy Solutions, University of South Africa, Florida Campus, Johannesburg 1710, South Africa

[4] Microscopy and Microanalysis Unit, University of the Witwatersrand, Johannesburg, South Africa

[5] Centre for High Resolution Transmission Electron Microscopy, Nelson Mandela University, Gqeberha 6031, South Africa

1 Introduction

Carbon dots (CDs) are a more recent class of carbon nanomaterials with excellent electronic properties, and they can act as electron donors or acceptors [1]. CDs are defined as quasi-spherical nanoparticles made up of an amorphous to nano-crystalline graphite core with sizes less than 10 nm [2, 3]. Since their discovery, many papers have been written about their synthesis and uses in different applications, including drug delivery, sensing, catalysis, and electronics [4–9]. They have been of interest mainly due to their tunable fluorescent properties, biocompatibility, low toxicity, and abundant low cost sources [10, 11].

In catalysis, metal nanoparticles supported on carbons such as carbon nanotubes, graphene, and other shaped carbons, including CDs, have been shown to act as excellent heterogeneous catalysts in many organic transformation studies [12–15]. In many catalytic reactions using metal–carbon catalysts, the metal must be in a reduced state and thus the preparation of metal nanoparticles supported on carbons for use in hydrogenation reactions involves the use of both metal reducing and stabilizing agents, such as citric acid, hydrazine hydrate, sodium borohydride, etc. [1, 16, 17]. Some of the reducing agents used are toxic (e.g., hydrazine hydrate/sodium borohydride) and can also lead to metal particle agglomeration [2]. The use of these reducing agents can limit reactant hydrogenation, hence it is important to find alternative reducing agents that are environmentally friendly and can stabilize metal nanoparticles to prevent their aggregation [1, 18].

The CDs surface has been reported to act as both a "ligand" (capping agent) to stabilize small metal particles and a reducing agent to generate small metal agglomerates from metal ions [19–22]. Since the CDs are small (< 10 nm), this means that the interaction between the carbon and the metal will be unusual since both will have similar sizes. This can lead to the possibility of inverse catalyst-support interactions where the catalyst particle can be larger than the support particle [23]. Further, the CDs themselves can also act as catalysts or nanocomposite catalysts due to their ability to act as an electron donor or electron acceptor [7, 24]. To further investigate the dual effect of a metal and CDs, in particular when the metal particle is larger than the CD particle, we synthesized Pd-CDs composites and studied their behaviour (as well as that of the CDs) in the hydrogenation of cinnamaldehyde (CALD) as a model reaction.

Figure 1 shows the schematic representation of the selective hydrogenation of CALD. Hydrogenation of CALD results in the formation of three different products with hydrocinnamaldehyde (HCALD) and cinnamyl alcohol (CA) as intermediate products and 3-phenyl-1-propanol as a final product [25–27]. The products produced from this process are all industrially valuable and they are used for the synthesis of fine chemicals [26–29]. Selective hydrogenation of CALD is a challenge even though the hydrogenation of the C = C bonds relative to the C = O bonds is kinetically and thermodynamically more favourable [29–31].

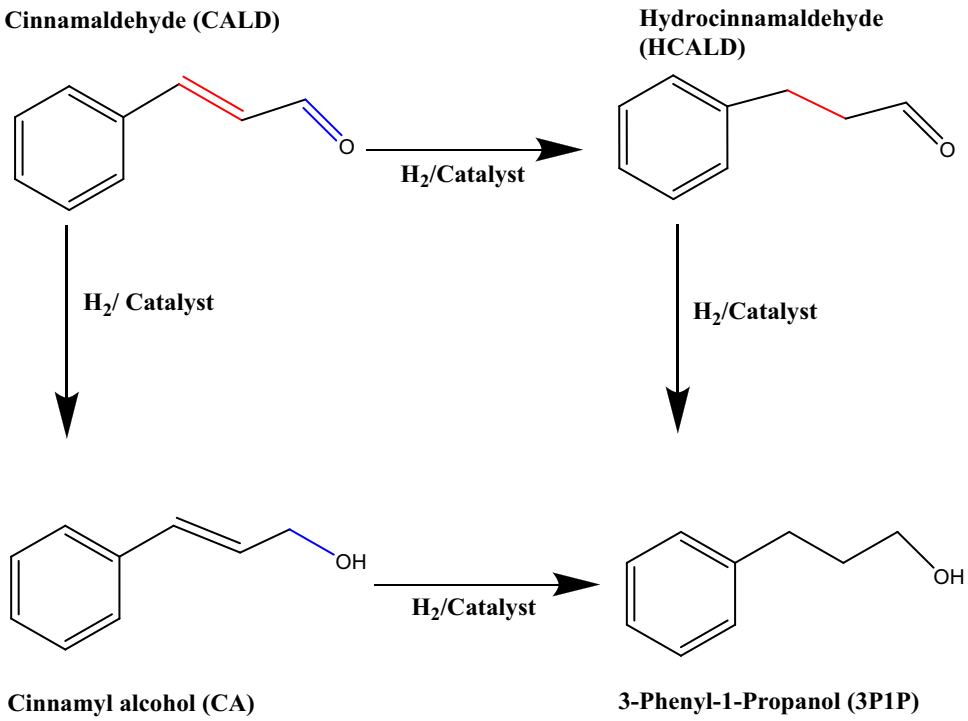

Fig. 1 Reaction pathway for the selective hydrogenation of CALD

We chose to generate a metal-CDs complex with Pd, as the Pd catalyst has been studied intensely in different organic transformation reactions [26, 32, 33]. Among these reactions, the use of Pd based catalysts for the hydrogenation of cinnamaldehyde has been well documented and provides a good model reaction for the study [33–39]. Studies have shown that the Pd catalyst is mostly selective towards the reduction of the C = C bond [40, 41].

The reduction of a Pd salt using CDs has been reported and the synthesized composites have been tested in many different applications including electrochemistry and photochemistry studies [41–43]. For example, Wei and Chen synthesized Pd nanoparticles supported on carbon nanodots (Pd-CDs) [21]. The Pd-CDs composite was applied as an anode catalyst for methanol oxidation in alkaline fuel cells. From the electrochemical measurements, the Pd-CDs catalyst displayed high electrochemical activity for methanol oxidation in alkaline electrolyte. It was also noted that the catalyst provided non-blocked active surfaces for the fuel oxidation reaction.

Pd-CDs composites have also been used in classic organic synthesis type reactions. Dey et al. investigated the catalytic effect of carbon dot reduced palladium nanoparticles (Pd@CDs) for Suzuki-Miyuara and Heck coupling reactions [20]. The authors found that the CDs did not have much impact on the prevention of Pd nanoparticle agglomeration. The catalytic activity of the catalyst, referred to as Pd@CDs, for the coupling of phenylboronic acid and bromobenzene reached a maximum conversion of 45% to biphenyl after 10 h. The catalyst started to deactivate and precipitation of a Pd@CDs composite (Pd within a sheet like carbon) was observed during the reaction.

The present work reports for the first time the use of CDs and Pd-CDs catalysts in the liquid phase hydrogenation of CALD. The catalytic activity and selectivity of the two catalysts were investigated. It was found that the two catalysts had different activity and selectivity in the hydrogenation of CALD. Transmision electron microscopy results indicated that in the presence of the Pd, the CDs were converted into carbon sheets at a low temperature (< 100 °C). Catalyst deactivation was observed, and this was related to the conversion of the CDs to carbon sheets, which permitted Pd agglomeration. This study indicates the limitation of using Pd supported on CDs in catalytic reactions due to the conversion of the CDs to carbon sheets by Pd ions.

2 Experimental Procedure

The methods used to synthesize CDs and the Pd-CDs composite were modified from the methods reported in the literature by Chen et al. [44] and Dey et al. [20] respectively.

2.1 Materials

The chemicals used were of technical and analytical grade. Sucrose, oleic acid (90%), CALD (98%), CA (98%), 3P1P (98%, FCC), HCALD (90%) and $PdCl_2$ (99%) were purchased from Sigma-Aldrich. The absolute ethanol was purchased from MK chemical. Hexane fraction and HCl (32%) were purchased from Associated Chemical Enterprise.

2.2 Synthesis and Surface Reaction of Carbon Dots

CDs were synthesized by refluxing 20 g of sucrose and 20 mL of oleic acid for 2½ h at 215 °C under a nitrogen atmosphere. After cooling the supernatant liquid was discarded and the brown solid product at the bottom of the flask was dispersed in 40 mL distilled water. The CDs were then extracted using hexane and water to remove the remaining oleic acid. The final product was oven-dried for 72 h at 100 °C. The yield of the CDs (brown solid) obtained was 41%.

Surface functionalization of the CDs was carried out as follows: 500 mg of the as-synthesized CDs was dispersed in 100 ml acetic acid (90%). The resulting solution was refluxed at 90 °C for 1 h. After refluxing, the solvent was evaporated at 70 °C and then washed with water. The functionalised CDs (fCDs) were dried in the oven at 100 °C for 24 h.

2.3 Synthesis of 1 wt. % Pd-CDs

CDs (100 mg) were dispersed in distilled water (100 mL) followed by the addition of 3.75 mL of 2 mM H_2PdCl_4. The mixed solution was refluxed at 100 °C for 6 h. The resultant solution was evaporated using a rotary evaporator at 70 °C. The product was washed several times using ethanol. The nanoparticles were oven-dried for 48 h at 100 °C.

2.4 Characterization of Materials

The catalyst loading was determined by inductively coupled plasma-emission spectroscopy (ICP-OES), which was carried out using a Spectro Arcos ICP-OES. The morphology of the CDs and Pd-CDs composite was analyzed by high resolution transmission electron microscopy (HRTEM) using a Tecnai G2 30ST operating at 200 kV and high-angle annular dark field imaging (HAADF). The Pd and CDs particle sizes were measured using Image J software by counting > 100 particles from TEM images obtained. Scanning transmission electron microscopy (STEM) images were acquired using a JEOL ARM-200F operating at 200 kV. The phase composition of the prepared samples was determined using, a Bruker D_2 phaser PXRD equipped with a Lynxene detector using Cu-K_α ($\lambda = 1.54184$ Å) radiation at 30 kV with a scan range

from $5° \leq 2\,\Theta \leq 90°$ in 0.026 steps. The thermal stability of the samples was determined using a Perkin Elmer thermogravimetric analyser (TGA 4000) in air in the temperature range of 35–900 °C (10 °C/min). The presence of functional groups on the surface of the samples was determined using a Brüker Tensor 27 Fourier transform infrared (FTIR) spectrometer. UV–vis absorption measurements were carried out using a Varian Cary Eclipse (Cary 50) UV–vis absorption spectrophotometer. Photoluminescence characteristics were measured using an Agilent Cary Eclipse fluorescence spectrometer. The Raman spectra were recorded using a Bruker Senterra Raman spectrophotometer with a laser wavelength of 532 nm using Opus 7.1 software. The elemental composition of the samples was determined using X-ray photoelectron spectroscopy (XPS) using a Thermo ESCAlab 250Xi equipped with a monochromatic Al K_α X-ray source operating at 1486.7 eV.

2.5 Catalytic Tests

The selective hydrogenation of CALD was carried under atmospheric pressure in a three-neck round bottom flask (100 mL) equipped with a condenser, magnetic stirrer, gas inlet, and sampling port. The three-neck round bottom flask was placed inside an oil bath with a thermocouple to maintain the desired temperature. The reaction mixture consisted of 100 mg catalyst, 1.32 g CALD, and 100 mL absolute ethanol. To remove traces of dissolved oxygen, N_2 gas was bubbled into the reaction mixture while the temperature was ramped to 60 °C (2 °C/min). Once the oil bath reached 60 °C, N_2 was switched with H_2 (50 mL/min) gas to allow for the hydrogenation of CALD. The reaction was carried out for 7 or 8 h while taking samples of the reaction periodically for analysis.

Product analysis was carried out using an offline Varian 3700 GC with a flame ionization detector (FID) and a capillary column (Phenomenex Zebron, 30 m L. × 0.53 mm I.D. × 1.5 μ F.T.). The conditions for analysis were as follows: the temperatures for the column, detector and injector were set to 300, 250, and 200 °C respectively, with N_2 (5 mL/min) as the carrier gas.

3 Results and Discussion

3.1 Synthesis and Characterization of CDs

The synthesis of the CDs was performed using a variation of a classical procedure to make very small CDs [44]. The CDs were fully characterized by HRTEM, TGA, XRD, FTIR, XPS, UV–vis and PL spectroscopy and their properties are comparable to the CDs made by Chen and co-workers [44] (Figs. 2, 3, S1, S2 and S3). Figure 2a shows the high magnification TEM image of the CDs with an average particle size of 0.9 ± 0.4 nm (Fig. 2b). A small shift in the PL maxima (Fig. S3b) from 471 to 461 nm when compared to CDs reported by Chen and co-workers [44] is consistent with the smaller particles produced in this study [45].

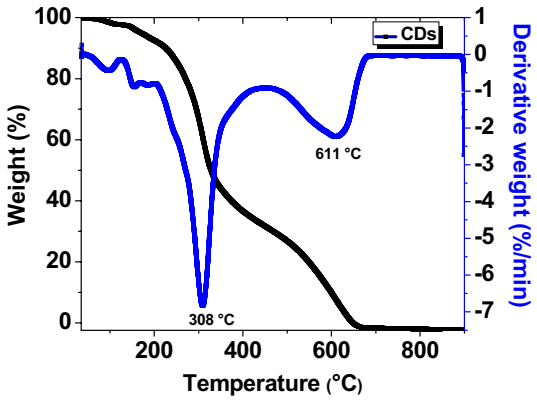

Fig. 3 TGA and the DTG profile of the CDs

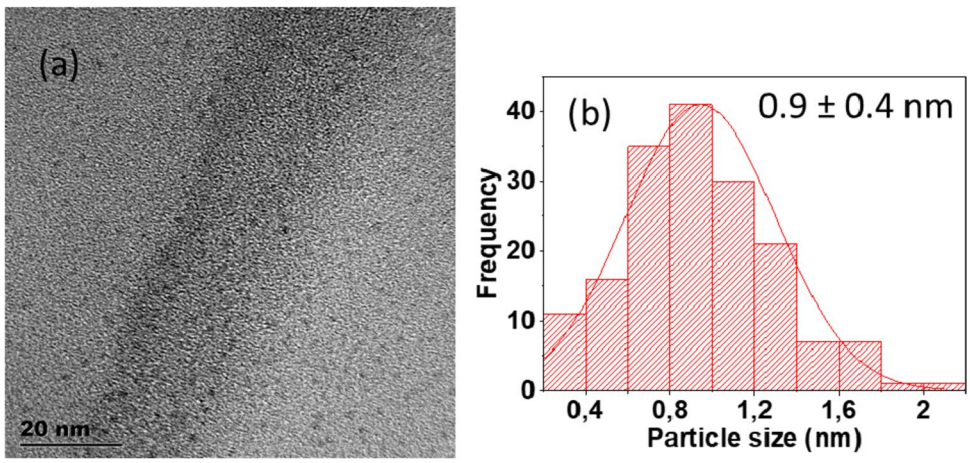

Fig. 2 **a** High magnification TEM image and **b** particle size distribution of the CDs

The thermal stability of the CDs was determined by using TGA and the CDs gave a classic weight loss expected for CDs (Fig. 3). The first and second small decomposition peaks at around 95–155 °C can be attributed to the loss of adsorbed moisture as the CDs are known to be hygroscopic [46, 47]. The onset decomposition temperature of the oxygen-containing functional groups and amorphous carbon was 223 °C with a maximum loss in the derivative curve at 308 °C. The weight percentage of amorphous carbon containing surface functional groups was estimated to be 56.6%. The decomposition peak of the core carbon of the CDs was observed in the TG derivative curve at ca. 611 °C. This indicates that the core carbon of the CDs is a graphitic type of carbon.

3.2 Synthesis of the Pd-CDs Composite

The Pd-CDs were made by reducing Pd salt using CDs without the addition of any other reducing agent. The Pd metal content on the synthesized Pd-CDs catalyst was determined using ICP-OES and was found to be 0.81 wt. % Pd. A TEM image of the Pd NPs is shown in Fig. 4a and the NPs have variable sizes (5.5–13.7 nm). The Pd NPs had an average particle size of 9.3 ± 3.7 nm (Fig. S4c). To show if there is any interaction between the Pd NPs and CDs in the composite, a TEM image of the catalyst was taken at a slightly lower magnification, and it was noted that some of the Pd NPs are covered (embedded) with a carbon layer (Fig. S4a (red circle), b) whereas other NPs are not coated (blue circle). It appears that the Pd is seen on/in a carbon overlayer, similar to that described by Dey et al. [20], Dhenadhayalan et al. [48], and Chandrasekaran et al. [49]. The HRTEM image in Fig. 4b shows one of the large nanoparticles in the Pd-CDs composite. Here a multi-twinned Pd nanoparticle (d = 11.6 nm) with high crystallinity and a lattice *d*-spacing of 0.22 nm is seen. This lattice *d*-spacing corresponds to the (111) plane of Pd (0) and indicates that the Pd has been reduced by the CDs. A BF and HAADF STEM image of the sample (Fig. 4c, d) confirmed the presence of Pd and that the Pd NPs had variable diameters. No CDs were observed although carbon was detected as a sheet like material (Fig. S4). Thus, the TEM data reveals that a Pd-carbon

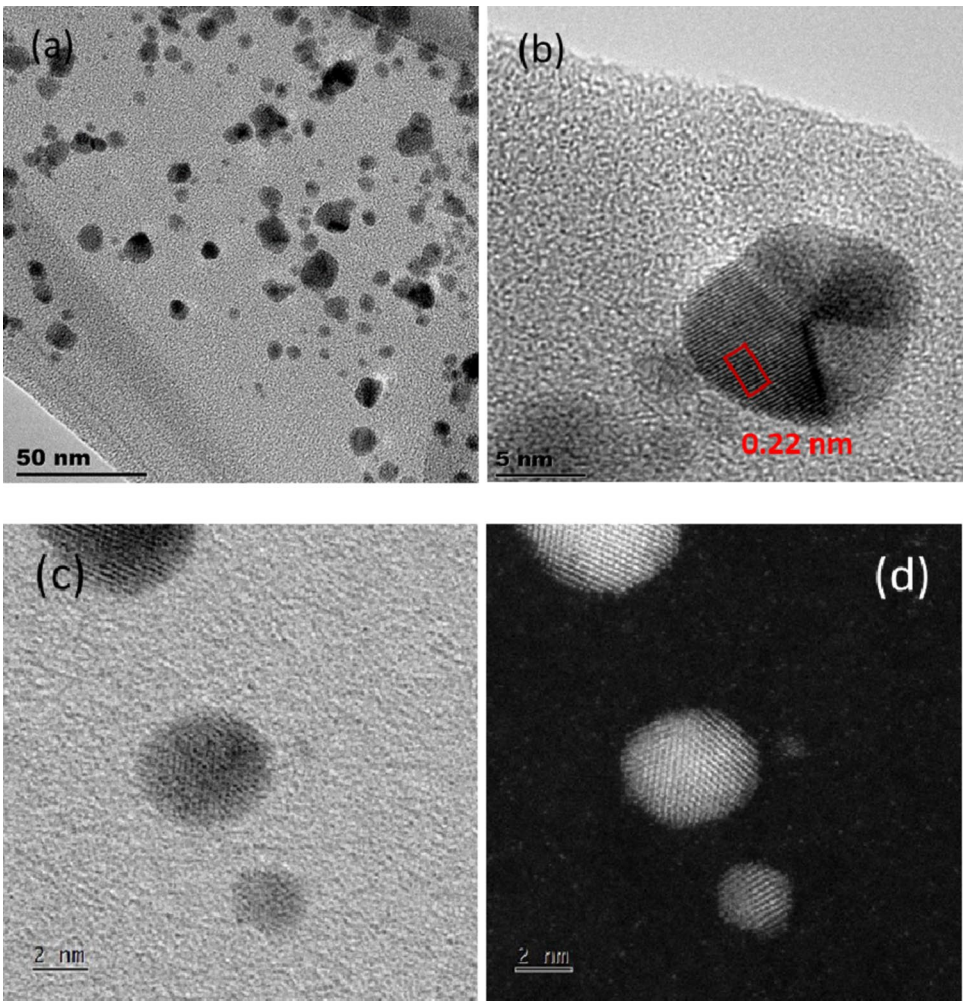

Fig. 4 **a**, **b** HRTEM images and **c**, **d** BF and HAADF STEM images of 1 wt. % Pd-CDs

catalyst has been made, and that the expected inverse catalyst support interaction was not observed; rather the CDs had been modified by the Pd [23, 50].

To determine if the Pd was responsible for the conversion of the CDs to carbon sheets during the reduction reaction, CDs (without Pd) were annealed under nitrogen at 190 and 300 °C for 10 min and 1 h, respectively (Fig. S5). At 190 °C only agglomeration of the CDs was observed but the carbon sheets were formed when the annealing temperature was increased to 300 °C. This is consistent with recent data that indicated CDs conversion to carbon nanosheets at high temperatures [51, 52]. It thus appears that the Pd reduced the temperature at which the CDs conversion produced sheets. The reaction in the presence of Pd occurred at T < 100 °C. The reduction of a metal by CDs functional groups is a common reaction, but conversion of the carbon core (by reduction) has been less studied. Indeed, a consideration of the reduction of metal oxides by carbon, as seen in Ellingham diagrams, indicates that easy to reduce metal oxides (ions) can achieve this conversion reaction [53].

Table S3 summarizes the work done using Pd-CDs composite in different reactions and indicates that indeed the Pd-CDs mixtures readily produce Pd-carbon sheet materials. It is thus clear from the data that the products produced in the reaction depends on the temperatures (i) used to add the Pd to the CDs and (ii) to study the Pd-CDs composite catalytic reactions. The reaction conditions determine the type of catalyst that is formed between Pd and the CDs (Pd-CDs inverse catalyst or Pd/carbon sheet) [20, 41, 44, 48, 49, 54, 55].

The PXRD data for the Pd-CDs composite also confirmed that the H_2PdCl_4 salt had been reduced to metallic Pd. The PXRD (Fig. 5a) peaks at *ca.* 39.7°, 46.3°, 67.1°, and 81.1° correspond to the Pd nanoparticle crystal planes: (111), (200), (220), and (311) [56]. The Pd nanoparticle plane (111) was more prominent than other phases which correlate to the lattice *d*-spacing obtained from HRTEM images of the Pd-CDs. The Pd crystallite size measured using the Scherrer equation gave d = 9.7 nm, a value similar to that found from TEM measurements. The thermal stability of Pd-CDs was studied using TGA (Fig. 5b). From the TGA, a residue of 0.45 wt. % (due to oxidized Pd) was observed. Compared to the TGA of the CDs, it was observed that the addition of the Pd catalyst decreased the thermal stability of the CDs. The presence of Pd also affected the removal of the functional groups with the maximum peak position reduced from 308 °C (see Fig. 3) to 186 °C. A small peak at *ca.* 300 °C is thought to be due to CDs that did not interact with Pd. The decomposition of the CDs core was observed in the derivative curve at *ca.* 424 °C, much lower than seen in the CDs. The early onset oxidation of the carbon can be attributed to the ability of the Pd nanoparticles to catalyze the oxidation of carbon [57]. The content of surface functional groups was also lower in the Pd-CDs as indicated by the ratio of the functional group/core carbon peaks (from 57% to 23.2%).

The UV–vis spectra (Fig. 6a) of the Pd-CDs composite is similar to that of the CDs with a small blue shift in the two absorption peaks (226 to 222 nm and 284 to 283 nm, CDs → Pd-CDs respectively). The absence of the plasmonic peaks for Pd (II) at 325 and 440 nm shows that a complete reduction of Pd (II) to Pd (0) has occurred [58, 59]. The addition of Pd to the CDs led to quenching of the photoluminescence of the CDs and shifted the peak maximum from 471 to 456 nm (Fig. 6b). This phenomenon can be attributed to possible aggregation of CDs, the removal of the CDs functional groups, and photoinduced electron transfer from the CDs shells to the metal core [60].

The FTIR spectrum (Fig. S7a) of the Pd-CDs showed little change from the CDs spectrum. However, XPS data (Fig. S7b) of the Pd-CDs showed that after the reduction of H_2PdCl_4 there was a decrease in the O1s atomic % of Pd-CDs composite from 26.8 to 22.4% when compared to the CDs (Fig. S2b). The C/O atomic ratio of Pd-CDs

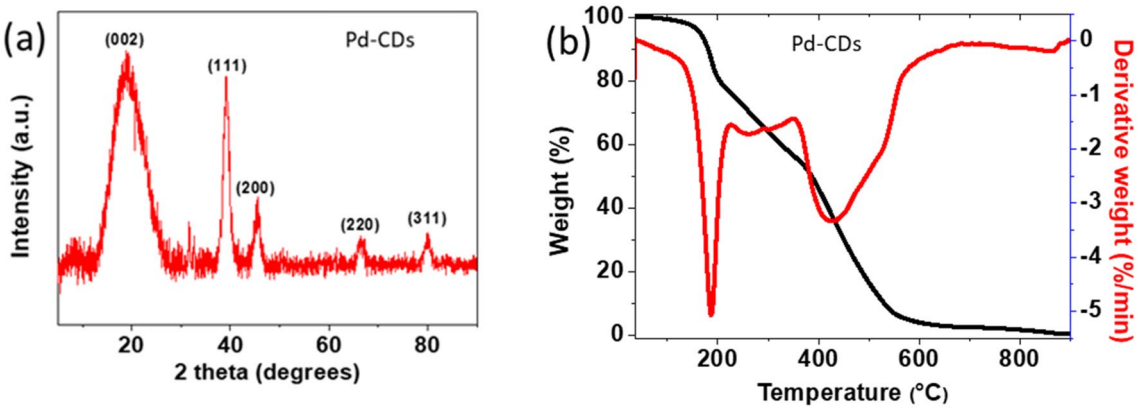

Fig. 5 **a** PXRD and **b** TGA and DTG of 1 wt. % Pd-CDs catalyst

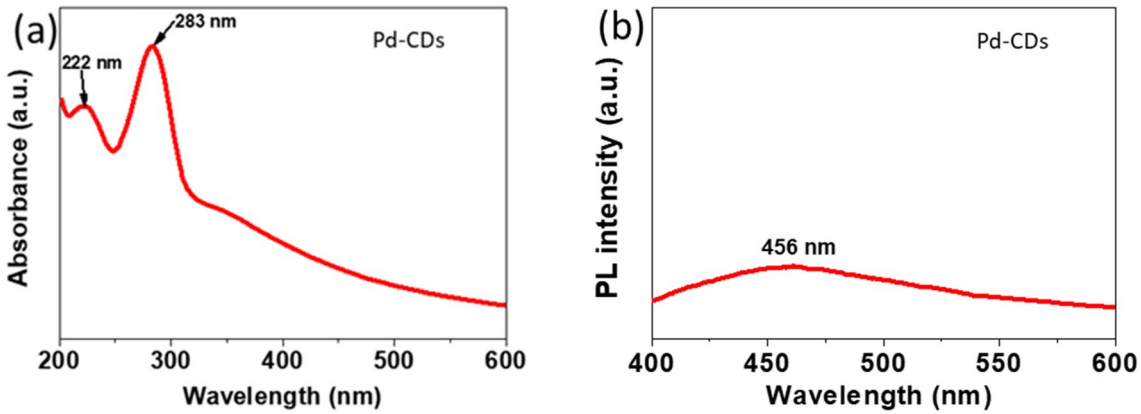

Fig. 6 **a** UV–vis spectra and **b** PL spectra of the 1 wt. % Pd-CDs catalyst

Table 1 Comparison of the atomic % of the oxygenated functional in C1s spectra of CDs and Pd-CDs

Sample	Pd-CDs		CDs	
C1s	BE (eV)	Atomic %	BE (eV)	Atomic %
C-O	285.9	11.0	286.1	20.9
C=O	287.1	2.5	287.3	4.5
O-C=O	288.4	1.1	288.5	4.6

composite was calculated to be 3.0 and this value is higher than that of the CDs (2.7). The deconvolution of the C1s XPS spectrum (Fig. S7c) of the Pd-CDs composite, as with the CDs, showed 5 types of carbon species which peaks in the spectrum correspond to C–C sp^2 (284.1 eV), C–C sp^3 (285.0 eV), C-O (285.9 eV), C=O (287.1 eV), O-C=O (288.4 eV) indicating that the composite still has oxygenated functional groups. A decrease in the intensity of the oxygenated peaks (C=O, O-C=O, and C-O) on the surface of the CDs was also observed. These small changes relate to the small amount of Pd used in the reaction; larger amounts give larger effects. This reduction in the intensity of the oxygenated peaks was also observed by Dey et al. [20].

From the XPS and FTIR data of both CDs and Pd-CDs, it can be noted that there are changes in the surface functional groups of the CDs. The reduction in the intensity and shifts in the wavenumbers of the oxygenated functional groups in the IR spectra can be ascribed to the transfer of electrons that occurred during the reduction of Pd ions to metallic Pd [20, 49, 50, 62, 63]. This can be supported by the XPS data where a large decrease in atomic % of C-O peaks in the C1s spectra of Pd-CDs (Table 1) is observed. The oxygenated functional groups have also been reported to serve as nucleation centres for the growth of Pd NPs which, then leads to the transformation of the CDs to carbon sheets [62, 63].

In summary, the method used in the synthesis of the Pd-CDs resulted in the Pd ions/oxide being reduced by the CDs and some interaction between the CDs and Pd was shown (TGA, UV–vis, PL spectroscopy). Further, the interaction of the CDs with the Pd led to the partial removal of surface groups by the Pd and the conversion of the CDs to a carbon layered material. The observation of the conversion of CDs to carbon sheets has been described before, but in the literature report, the reaction occurred thermally at temperatures > 200 °C [51]. In other studies CDs conversion into porous 3D carbon framework thermally at high temperatures has also been mentioned [64]. It appears from our study that this reaction to convert CDs to other carbon shapes can also occur at lower temperatures (100 °C) in the presence of the Pd acting as a catalyst. The reaction resulted in coverage/embedding of the Pd with a carbon overlayer that was generated from the CDs, as seen by others [20, 48, 49]. The process by which this conversion occurs is still not known in any detail.

3.3 Hydrogenation of CALD Using CDs and Pd-CDs Composite

3.3.1 Catalytic Reactions of CDs

Carbon materials are known to act as catalysts, a phenomenon known as carbocatalysis [65, 66]. The development of carbon nanomaterials (CNMs) such as fullerene, CNTs, graphene, nanodiamonds, and mesoporous carbon has led to an enormous interest in the use of these CNMs as carbocatalysts in various catalytic applications [67]. Functional groups on the surface of these CNMs have been identified as one of the catalytic sites [67–69].

The CALD hydrogenation reaction was carried out in the liquid phase. The catalytic activity of the CDs towards the hydrogenation of CALD was evaluated at 40 and 60 °C (Fig. 7). The reaction is in general rapid, and the reaction terminated prior to conversion of all the CALD. For example, at 60 °C within 4 h 40% CALD conversion was obtained,

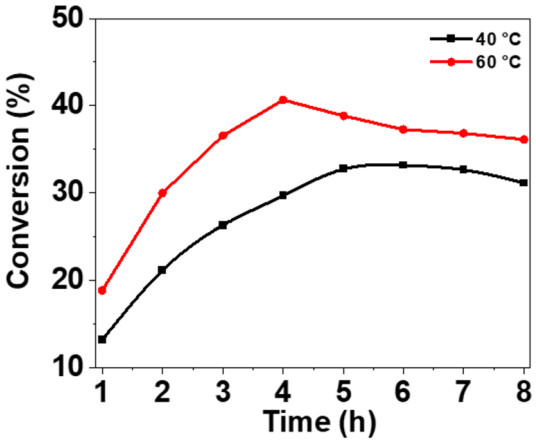

Fig. 7 The conversion of CALD over CDs catalyst at 40 °C and 60 °C (50 mg CDs, 50 mL/min = H_2 flow rate, 100 ml ethanol, and 1.32 g CALD)

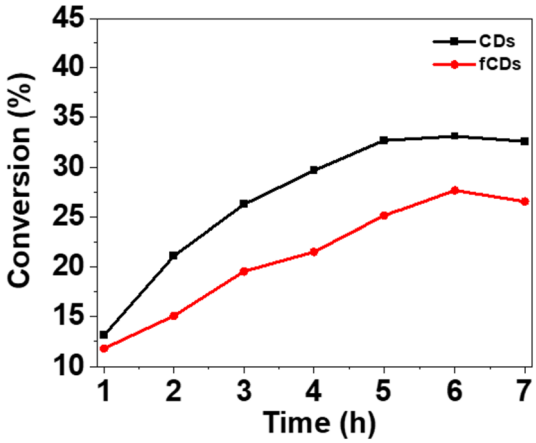

Fig. 8 Conversion of CALD over CDs and fCDs catalysts at 40 °C. Reference conditions: $m_{catalyst}$ = 50 mg, t = 7 h, 50 mL/min = H_2 flow rate, 100 ml ethanol, and 1.32 g CALD

and after that no further reaction took place. In terms of selectivity, the CDs catalyst was completely selective to the hydrogenation of the C = O bond forming CA, and no HCALD and 3P1P were detected. This is consistent with the ability of the carbon π-electrons to donate electrons to the CALD, as observed for Pt which also hydrogenates the C = O bond [70].

In an attempt to modify the activity of the CDs, a surface reaction with acetic acid (to give fCDs) was undertaken to generate potential reaction sites. The FTIR spectrum (Fig. S8a) of the fCDs indeed showed the growth of peaks at 3366, 1711, and 1018 cm^{-1} which corresponds to O–H, C = O, and C–O–C functional groups when compared to the FTIR spectrum of the CDs. There was also a slight red shift in the peaks suggesting stronger bond formation (Table S1). The fCDs were used in the cinnamaldehyde reduction reaction, and the fCDs gave a reduction in catalyst activity indicating that the acid functional groups were not the major contributor to the reaction (Fig. 8). The selectivity to C = O reduction was maintained.

3.3.2 Catalytic Activity of Pd-CDs

The catalytic activity of the Pd-CDs catalysts was determined. The activity was found to be higher for the Pd-CDs than for the CDs but also, significantly, the product distributions were entirely different (it is to be noted that the Pd content was < 1 wt. %). For example, after 1 h reaction using similar reaction conditions (60 °C) the conversion of CALD was higher for the Pd-CDs (28.4%) than for the CDs (18.8%) (Table 2). Thus, the Pd-CDs catalyst completely overwhelmed the catalytic reaction of the carbon sheets made from the CDs. This suggests that the reduction of the Pd by the CDs removed the active surface groups responsible for the hydrogenation of the CALD to CA.

The catalytic activity of Pd-CDs catalyst was further studied, using different reaction conditions. The effect of the Pd-CDs catalyst mass on the hydrogenation of CALD was tested at 60 °C (Fig. 9). A relatively good linear correlation between the catalyst activity and the amount of catalyst used was observed. The conversion of CALD increased from 46 to 73% with an increase in the catalyst mass.

The effect of reaction temperature on the CALD conversion and product selectivity was also studied by varying the temperature between 40 and 80 °C (Fig. S9). The activity (mol/g_{Pd}.h) based on CALD conversion towards the Pd mass on the Pd-CDs catalyst was calculated. Figure 10 shows the effect of temperature on the catalyst activity after 1 h. The catalyst activity increased from 7.2 to 8.2 mol/g_{Pd}.h with increasing reaction temperature. As the reaction temperature increased the turnover number of the effective active sites of the catalyst slightly increased. The catalyst was 100% selective toward the reduction of the C = C bond, forming only hydrocinnamaldehyde.

Figure 11 shows the influence of H_2 flow rate on the hydrogenation of the CALD over the Pd-CDs catalyst. An

Table 2 CDs and Pd-CDs activity and selectivity for the hydrogenation of CALD

Catalysts	Conversion (%)	Selectivity (%)		
		HCALD	3P1P	CA
CDs	18.8	0	0	100
Pd-CDs	28.4	100	0	0

Reference conditions: 1 h, 50 mg catalyst, 50 mL/min = H_2 flow rate, 100 ml ethanol, T = 60 °C, and 1.32 g CALD

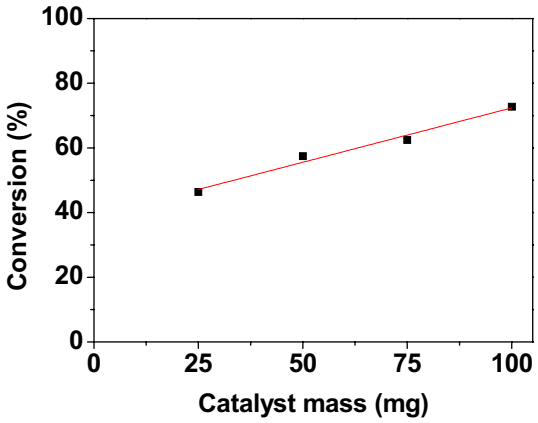

Fig. 9 The conversion of CALD over Pd-CDs catalyst. Reference conditions: T = 60 °C, t = 7 h, 50 mL/min = H_2 flow rate, 100 ml ethanol, and 1.32 g CALD

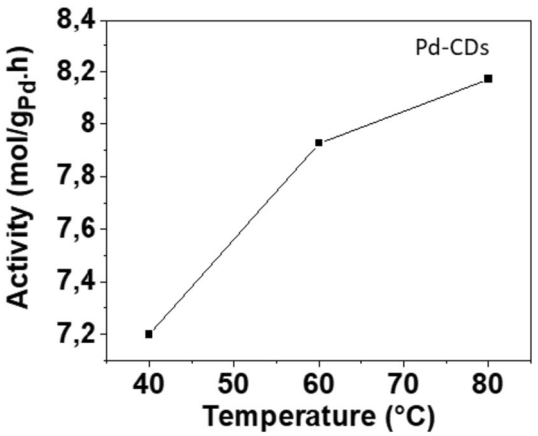

Fig. 10 Effect of temperature on the activity of the Pd-CDs catalyst

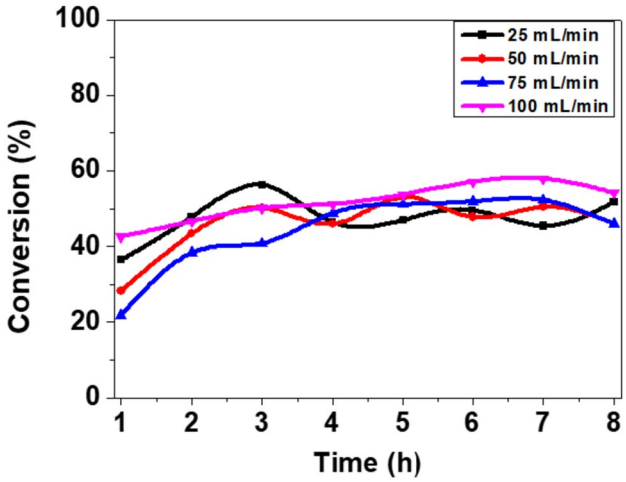

Fig. 11 The conversion of CALD over the Pd-CDs catalyst at different hydrogen flow rates. Reference conditions: T = 60 °C, 50 mg catalyst, 100 ml ethanol, and 1.32 g CALD

increase in the hydrogen flow rate did not have a significant influence on the activity of the catalyst and did not change the selectivity of the catalyst.

Recyclability studies were undertaken; the catalyst from a previous reaction was separated from the reaction medium using a centrifuge and washed using ethanol. The obtained catalyst was dried at 100 °C for 2 h. To reactivate the catalyst, it was reduced at 190 °C using a CVD furnace under a flow of H_2 (50 ml/min) and N_2 as a carrier gas. The data indicated that the catalysts lost activity completely after the first cycle.

TEM images were recorded on the catalyst after the reaction (Fig. 12). A comparison of Figs. 4a and S4 with Fig. 12 indicates that three effects have occurred: (i) the Pd particles have agglomerated further (ii) the carbon particles have now formed thicker sheets and (iii) the carbon appears to have encapsulated the Pd. These multiple effects led to the deactivation of the catalyst. It is clear that the CDs thus play no role in stabilizing the Pd particles as was also observed in the study conducted by Dey et al. [20].

3.3.3 Comments on the Mechanism

In the literature, the product selectivity of metal catalysts has been associated with the metal d-band width [35, 71]. The metal d-band width can be arranged in the following increasing order: Pd < Pt < Ir ≈ Os [35]. The chances of the metal surface interacting with the conjugated C = C bond increases with a narrower d-band metal width suggesting that Pd would catalyse the C = C bond in CALD [35].

Our initial objective was to investigate the role of Pd supported on CDs to study an inverse catalyst support effect ($d_{Pd} > d_{support\ particle}$) and to study the selectivity of this type of catalyst. The first step was to evaluate the CDs in the CALD hydrogenation reaction. Here studies showed that the C = O bond was selectively hydrogenated. Functionalization of the CDs with acetic acid further revealed that the acid C = O groups were not the dominant groups required to hydrogenate the C = O CALD bond.

The Pd-CDs composite was then investigated for the CALD hydrogenation. After the reduction of the Pd salt using CDs, changes in the surface chemistry of the catalyst were noted. In particular, the CDs were converted into carbon sheets, thus the new catalyst was rather made of Pd embedded in, or on top of, the sheets.

This suggest that the Pd has the ability to convert the CDs into sheets in solution at low temperature. The data are indeed consistent with other reports in which Pd-CDs have revealed lack of a typical CD structure after Pd reduction. The partial removal of the functional groups during the reduction of the Pd salt thus allows for 'stitching together' of the carbons to form the sheets. The effect has also been seen during high temperature annealing. Thus, the data indicate

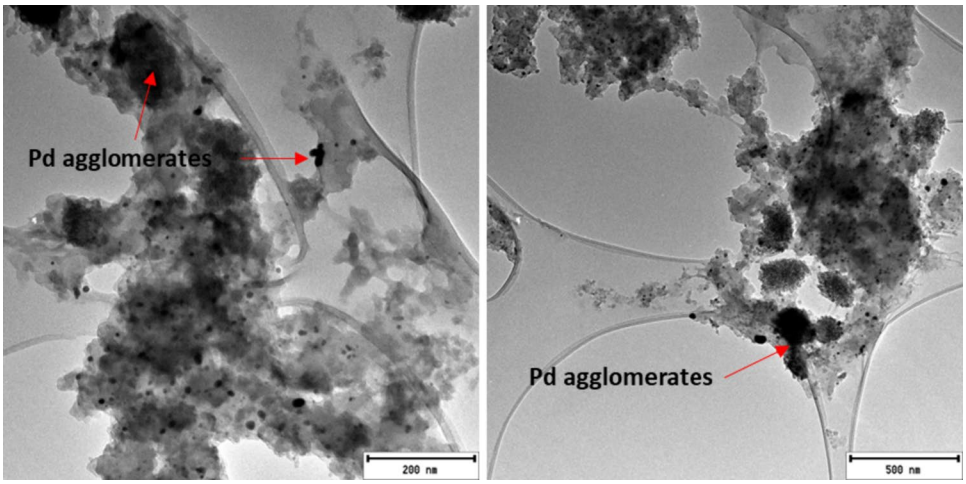

Fig. 12 TEM images of the Pd-CDs catalyst after first catalyst cycle

that Pd readily converts CDs into sheet like and layered carbons. Similar observations were found when reducing other metals like silver [71] and gold [19, 72] using CDs.

The conversion of the CDs suggested that the activity of the CDs was modified by this process due to i) loss of surface area and ii) loss of functional groups. The study indicated that the Pd (< 1%) then dominated the catalytic reaction. We assume that the active functional groups responsible for the selectivity towards the C = O bond were removed from the CDs during the reduction of the Pd salt. Toebes et al. has also reported that the removal of the oxygenated functional groups present on a Pt/carbon nanofibres catalyst resulted in an enhanced selectivity towards the reduction of the C = C bond in the hydrogenation of CALD [73].

4 Conclusions

The data presented from this study shows that CDs can be used as a reducing agent for Pd salts thus avoiding the use of strong and toxic reducing agents. From HRTEM studies, it was shown that highly crystalline Pd NPs were formed after reaction of a Pd salt with the CDs. The UV–vis spectra of the Pd-CDs is similar to that of CDs and no plasmonic peaks of Pd (II) were observed. The PL and Raman spectra of the Pd-CDs catalyst has shown that CDs have electron transfer properties indicated by quenching of the photoluminescence of the CDs. The interaction between CDs and Pd NPs is similar to reactions with other nano carbons in which the Pd salts are reduced by the carbon.

The use of the Pd-CDs catalyst for the reduction of CALD led to a conversion of 78% at 80 °C. It was observed that the CDs and Pd-CDs catalysts favoured different adsorption modes (C = O or C = C respectively) leading to different product distributions A significant finding from the study, that explained the catalytic data, related to the Pd catalyzed conversion of the CDs into carbon sheets. This occurred in solution at low temperature. The sheet formation resulted in Pd agglomeration, which was used to rationalise the catalyst deactivation observed in the reaction.

The data show that care needs to be used when CDs are used as supports, even in low temperature reactions, when easy to reduce metal ions are used as catalysts. The CDs have the ability to convert into other shapes under the reaction conditions, and this will impact in the agglomeration and hence the activity of the catalysts.

Supplementary Information The online version contains supplementary material available at https://doi.org/10.1007/s10562-023-04540-7.

Acknowledgements We acknowledge the NRF, the DSI-NRF Centre of Excellence in Strong Materials (CoE-SM) and the University of the Witwatersrand (Postgraduate Merit Award) for funding. We thank Prof A. Ziegler and Dr. L. Mokoloko (both from the University of the Witwatersrand) for useful discussions.

Funding Open access funding provided by University of the Witwatersrand.

References

1. Zhang J, Chen Y, Tan J et al (2017) The synthesis of rhodium/carbon dots nanoparticles and its hydrogenation application. Appl Surf Sci 396:1138–1145. https://doi.org/10.1016/j.apsusc.2016.11.101

2. Đorđević L, Arcudi F, Cacioppo M, Prato M (2022) A multifunctional chemical toolbox to engineer carbon dots for biomedical and energy applications. Nat Nanotechnol 17:112–130. https://doi.org/10.1038/s41565-021-01051-7
3. Liu Y, Huang H, Cao W et al (2020) Advances in carbon dots: from the perspective of traditional quantum dots. Mater Chem Front 4:1586–1613. https://doi.org/10.1039/D0QM00090F
4. Naik K, Chaudhary S, Ye L, Parmar AS (2022) A strategic review on carbon quantum dots for cancer-diagnostics and treatment. Front Bioeng Biotechnol 10:882100. https://doi.org/10.3389/fbioe.2022.882100
5. Dubey N, Dhiman S, Koner AL (2023) Review of carbon dot-based drug conjugates for cancer therapy. ACS Appl Nano Mater 6:4078–4096. https://doi.org/10.1021/acsanm.2c05407
6. Wang S, Chen H, Xie H et al (2021) A novel thioctic acid-carbon dots fluorescence sensor for the detection of Hg2+ and thiophanate methyl via S-Hg affinity. Food Chem 346:128923. https://doi.org/10.1016/j.foodchem.2020.128923
7. Dhenadhayalan N, Lin K, Saleh TA (2020) Recent advances in functionalized carbon dots toward the design of efficient materials for sensing and catalysis applications. Small 16:1905767. https://doi.org/10.1002/smll.201905767
8. Zhang P, Wei J-S, Chen X-B, Xiong H-M (2019) Heteroatom-doped carbon dots based catalysts for oxygen reduction reactions. J Colloid Interface Sci 537:716–724. https://doi.org/10.1016/j.jcis.2018.11.024
9. Semeniuk M, Yi Z, Poursorkhabi V et al (2019) Future perspectives and review on organic carbon dots in electronic applications. ACS Nano 13:6224–6255. https://doi.org/10.1021/acsnano.9b00688
10. Dubey P, Nimbalkar T, Sahu V, Bano S (2023) A review on synthesis and application of carbon quantum dots. Eur Chem Bull 12:1509–1518
11. Liu J, Li R, Yang B (2020) Carbon dots: a new type of carbon-based nanomaterial with wide applications. ACS Cent Sci 6:2179–2195. https://doi.org/10.1021/acscentsci.0c01306
12. Manjupriya R, Roopan SM (2021) Carbon dots-based catalyst for various organic transformations. J Mater Sci 56:17369–17410. https://doi.org/10.1007/s10853-021-06354-7
13. Rosso C, Filippini G, Prato M (2020) Carbon dots as nano-organocatalysts for synthetic applications. ACS Catal 10:8090–8105. https://doi.org/10.1021/acscatal.0c01989
14. Chen BB, Liu ML, Huang CZ (2020) Carbon dot-based composites for catalytic applications. Green Chem 22:4034–4054. https://doi.org/10.1039/D0GC01014F
15. Guan X, Li Z, Geng X et al (2023) Emerging trends of carbon-based quantum dots: nanoarchitectonics and applications. Small 19:2207181. https://doi.org/10.1002/smll.202207181
16. Suresh U, Subhadra S, Sivaramakrishnan S (2023) Green hydrothermal synthesis of carbon dot-silver nanocomposite from Chondrococcus hornemanni (marine algae): an application of mosquitocidal, anti-bacterial, and anti-cancer (MDA-MB-231 cells). Biomass Conv Bioref. https://doi.org/10.1007/s13399-023-04214-9
17. Ansi VA, Sreelakshmi P, Poovathinthodiyil R, Renuka NK (2021) Table sugar derived carbon dot—a promising green reducing agent. Mater Res Bull 139:111284. https://doi.org/10.1016/j.materresbull.2021.111284
18. Sun J-K, Xu Q (2015) Metal nanoparticles immobilized on carbon nanodots as highly active catalysts for hydrogen generation from hydrazine in aqueous solution. ChemCatChem 7:526–531. https://doi.org/10.1002/cctc.201402735
19. Wang X, Long Y, Wang Q et al (2013) Reduced state carbon dots as both reductant and stabilizer for the synthesis of gold nanoparticles. Carbon 64:499–506. https://doi.org/10.1016/j.carbon.2013.07.104
20. Dey D, Bhattacharya T, Majumdar B et al (2013) Carbon dot reduced palladium nanoparticles as active catalysts for carbon–carbon bond formation. Dalton Trans 42:13821. https://doi.org/10.1039/c3dt51234g
21. Wei W, Chen W (2012) "Naked" Pd nanoparticles supported on carbon nanodots as efficient anode catalysts for methanol oxidation in alkaline fuel cells. J Power Sources 204:85–88. https://doi.org/10.1016/j.jpowsour.2012.01.032
22. Im H, Noh S, Shim JH (2020) Spontaneous formation of core-shell silver-copper oxide by carbon dot-mediated reduction for enhanced oxygen electrocatalysis. Electrochim Acta 329:135172. https://doi.org/10.1016/j.electacta.2019.135172
23. Zhang J, Medlin JW (2018) Catalyst design using an inverse strategy: From mechanistic studies on inverted model catalysts to applications of oxide-coated metal nanoparticles. Surf Sci Rep 73:117–152. https://doi.org/10.1016/j.surfrep.2018.06.002
24. Dhenadhayalan N, Lin K-C (2020) Photochemically synthesized ruthenium nanoparticle-decorated carbon-dot nanochains: an efficient catalyst for synergistic redox reactions. ACS Appl Mater Interfaces 12:13759–13769. https://doi.org/10.1021/acsami.9b20477
25. Galvagno S, Capannelli G, Neri G et al (1991) Hydrogenation of cinnamaldehyde over Ru/C catalysts: effect of Ru particle size. J Mol Catal 64:237–246. https://doi.org/10.1016/0304-5102(91)85115-I
26. Zhao F, Ikushima Y, Chatterjee M et al (2003) An effective and recyclable catalyst for hydrogenation of α, β-unsaturated aldehydes into saturated aldehydes in supercritical carbon dioxide. Green Chem 5:76–79. https://doi.org/10.1039/b209252m
27. Zeng L, Yan H, Zeng Y et al (2019) Precious metal nanoparticles supported on KOH pretreated activated carbon under microwave radiation as a catalyst for selective hydrogenation of cinnamaldehyde. Can J Chem Eng 97:2505–2515. https://doi.org/10.1002/cjce.23487
28. Führer M, Van Haasterecht T, Bitter JH (2022) Cinnamaldehyde hydrogenation over carbon supported molybdenum and tungsten carbide catalysts. Chem Commun 58:13608–13611. https://doi.org/10.1039/D2CC05322E
29. Patil KN, Manikanta P, Srinivasappa PM et al (2023) State-of-the-art and perspectives in transition metal-based heterogeneous catalysis for selective hydrogenation of cinnamaldehyde. J Environ Chem Eng 11:109168. https://doi.org/10.1016/j.jece.2022.109168
30. Yuan T, Liu D, Pan Y et al (2019) Magnetic anchored CoPt bimetallic nanoparticles as selective hydrogenation catalyst for cinnamaldehyde. Catal Lett 149:851–859. https://doi.org/10.1007/s10562-018-2619-6
31. Prakash MG, Mahalakshmy R, Krishnamurthy KR, Viswanathan B (2017) Nickel based catalysts for selective hydrogenation of cinnamaldehyde- influence of support phases. ECB 6:125. https://doi.org/10.17628/ecb.2017.6.125-131
32. Bewana S, Ndolomingo MJ, Carleschi E et al (2019) Inorganic perovskite-induced synergy on highly selective Pd-catalyzed hydrogenation of cinnamaldehyde. ACS Appl Mater Interfaces 11:32994–33005. https://doi.org/10.1021/acsami.9b10820
33. Harada T, Ikeda S, Miyazaki M et al (2007) A simple method for preparing highly active palladium catalysts loaded on various carbon supports for liquid-phase oxidation and hydrogenation reactions. J Mol Catal A: Chem 268:59–64. https://doi.org/10.1016/j.molcata.2006.12.010
34. Sairanen E, Karinen R, Borghei M et al (2012) Preparation methods for multi-walled carbon nanotube supported palladium catalysts. ChemCatChem 4:2055–2061. https://doi.org/10.1002/cctc.201200344
35. Nagpure AS, Gurrala L, Gogoi P, Chilukuri SV (2016) Hydrogenation of cinnamaldehyde to hydrocinnamaldehyde over Pd

nanoparticles deposited on nitrogen-doped mesoporous carbon. RSC Adv 6:44333–44340. https://doi.org/10.1039/C6RA04154J
36. Pham-Huu C, Keller N, Ehret G et al (2001) Carbon nanofiber supported palladium catalyst for liquid-phase reactions. J Mol Catal A: Chem 170:155–163. https://doi.org/10.1016/S1381-1169(01)00055-3
37. Zhu J, Dou M, Lu M et al (2019) Thermo-responsive polymer grafted carbon nanotubes as the catalyst support for selective hydrogenation of cinnamaldehyde: effects of surface chemistry on catalytic performance. Appl Catal A: Gen 575:11–19. https://doi.org/10.1016/j.apcata.2019.02.009
38. Tessonnier J-P, Pesant L, Ehret G et al (2005) Pd nanoparticles introduced inside multi-walled carbon nanotubes for selective hydrogenation of cinnamaldehyde into hydrocinnamaldehyde. Appl Catal A: Gen 288:203–210. https://doi.org/10.1016/j.apcata.2005.04.034
39. Xu Z, Duong-Viet C, Liu Y et al (2019) Macroscopic graphite felt containing palladium catalyst for liquid-phase hydrogenation of cinnamaldehyde. Appl Catal B: Environ 244:128–139. https://doi.org/10.1016/j.apcatb.2018.11.041
40. Martínez-Ortiz MJ, De La Rosa-Guzmán MA, Vargas-García JR et al (2018) Selective hydrogenation of cinnamaldehyde using Pd catalysts supported on Mg/Al mixed oxides: Influence of the Pd incorporation method. Can J Chem Eng 96:297–306. https://doi.org/10.1002/cjce.22946
41. Duarah R, Karak N (2019) Hyperbranched polyurethane/palladium-reduced carbon dot nanocomposite: an efficient and reusable mesoporous catalyst for visible-light-driven C-C coupling reactions. Ind Eng Chem Res 58:16307–16319. https://doi.org/10.1021/acs.iecr.9b01805
42. Selim A, Kaur S, Dar AH et al (2020) Synergistic effects of carbon dots and palladium nanoparticles enhance the sonocatalytic performance for rhodamine B degradation in the absence of light. ACS Omega 5:22603–22613. https://doi.org/10.1021/acsomega.0c03312
43. Yan X, Li Q, Li L (2012) Formation and stabilization of palladium nanoparticles on colloidal graphene quantum dots. J Am Chem Soc 134:16095–16098. https://doi.org/10.1021/ja303730p
44. Chen B, Li F, Li S et al (2013) Large scale synthesis of photoluminescent carbon nanodots and their application for bioimaging. Nanoscale 5:1967. https://doi.org/10.1039/c2nr32675b
45. Wang Y, Hu A (2014) Carbon quantum dots: synthesis, properties and applications. J Mater Chem C 2:6921. https://doi.org/10.1039/C4TC00988F
46. Baker SN, Baker GA (2010) Luminescent carbon nanodots: emergent nanolights. Angew Chem Int Ed 49:6726–6744. https://doi.org/10.1002/anie.200906623
47. He Y, He J, Yu Z et al (2018) Double carbon dot assembled mesoporous aluminas: solid-state dual-emission photoluminescence and multifunctional applications. J Mater Chem C 6:2495–2501. https://doi.org/10.1039/C8TC00182K
48. Dhenadhayalan N, Hsin T, Lin K (2019) Multifunctional nanohybrid of palladium nanoparticles encapsulated by carbon-dots for exploiting synergetic applications. Adv Mater Interfaces 6:1900361. https://doi.org/10.1002/admi.201900361
49. Chandrasekaran P, Jebakumar Immanuel Edison TN, Sethuraman MG (2020) Electrocatalytic performance of carbon dots/palladium nanoparticles composite towards hydrogen evolution reaction in acid medium. Int J Hydrog Energy 45:28800–28811. https://doi.org/10.1016/j.ijhydene.2020.07.262
50. Janowska I, Ersen O, Jacob T et al (2009) Catalytic unzipping of carbon nanotubes to few-layer graphene sheets under microwaves irradiation. Appl Catal A: Gen 371:22–30. https://doi.org/10.1016/j.apcata.2009.09.013
51. Mokoloko LL, Matsoso BJ, Forbes RP et al (2021) Evolution of large-area reduced graphene oxide nanosheets from carbon dots via thermal treatment. Carbon Trends 4:100074. https://doi.org/10.1016/j.cartre.2021.100074
52. Luo H, Lari L, Kim H et al (2022) Structural evolution of carbon dots during low temperature pyrolysis. Nanoscale 14:910–918. https://doi.org/10.1039/D1NR07015K
53. Mokoloko LL, Forbes RP, Coville NJ (2023) The behavior of carbon dots in catalytic reactions. Catalysts 13:1201. https://doi.org/10.3390/catal13081201
54. Lin Z, Liu O, Guan S et al (2023) Self-crosslinked N-doped carbon dot supported Pd as an efficient catalyst for dehydrogenation of formic acid at room temperature. Sustain Energy Fuels 7:3096–3105. https://doi.org/10.1039/D3SE00407D
55. Gholinejad M, Bahrami M, Nájera C (2017) A fluorescence active catalyst support comprising carbon quantum dots and magnesium oxide doping for stabilization of palladium nanoparticles: application as a recoverable catalyst for Suzuki reaction in water. Mol Catal 433:12–19. https://doi.org/10.1016/j.mcat.2016.12.010
56. Huang Q, Lin X, Zhu J-J, Tong Q-X (2017) Pd-Au@ carbon dots nanocomposite: Facile synthesis and application as an ultrasensitive electrochemical biosensor for determination of colitoxin DNA in human serum. Biosens and Bioelectron 94:507–512. https://doi.org/10.1016/j.bios.2017.03.048
57. Moyo M, Motchelaho MAM, Xiong H et al (2012) Promotion of Co/carbon sphere Fischer-Tropsch catalysts by residual K and Mn from carbon oxidation by KMnO4. Appl Catal A: Gen 413–414:223–229. https://doi.org/10.1016/j.apcata.2011.11.012
58. Chen L-J, Wan C-C, Wang Y-Y (2006) Chemical preparation of Pd nanoparticles in room temperature ethylene glycol system and its application to electroless copper deposition. J Colloid and Interface Sci 297:143–150. https://doi.org/10.1016/j.jcis.2005.10.029
59. D'Souz L, Sampath S (2000) Preparation and characterization of silane-stabilized, highly uniform, nanobimetallic Pt−Pd particles in solid and liquid matrixes. Langmuir 16:8510–8517. https://doi.org/10.1021/la000496y
60. Luo P, Li C, Shi G (2012) Synthesis of gold@ carbon dots composite nanoparticles for surface enhanced Raman scattering. Phys Chem Chem Phys 14:7360. https://doi.org/10.1039/c2cp40767a
61. Hou H, Banks CE, Jing M et al (2015) Carbon quantum dots and their derivative 3D porous carbon frameworks for sodium-ion batteries with ultralong cycle life. Adv Mater 27:7861–7866. https://doi.org/10.1002/adma.201503816
62. Shen L, Chen M, Hu L et al (2013) Growth and stabilization of silver nanoparticles on carbon dots and sensing application. Langmuir 29:16135–16140. https://doi.org/10.1021/la404270w
63. De B, Karak N (2017) Recent progress in carbon dot–metal based nanohybrids for photochemical and electrochemical applications. J Mater Chem A 5:1826–1859. https://doi.org/10.1039/C6TA10220D
64. Navalon S, Dhakshinamoorthy A, Alvaro M, Garcia H (2014) Carbocatalysis by graphene-based materials. Chem Rev 114:6179–6212. https://doi.org/10.1021/cr4007347
65. Gordeev EG, Pentsak EO, Ananikov VP (2020) Carbocatalytic acetylene cyclotrimerization: a key role of unpaired electron delocalization. J Am Chem Soc 142:3784–3796. https://doi.org/10.1021/jacs.9b10887
66. Su DS, Wen G, Wu S et al (2017) Carbocatalysis in liquid-phase reactions. Angew Chem Int Ed 56:936–964. https://doi.org/10.1002/anie.201600906
67. Ma H, Wang L, Chen L et al (2007) Pt nanoparticles deposited over carbon nanotubes for selective hydrogenation of cinnamaldehyde. Catal Commun 8:452–456. https://doi.org/10.1016/j.catcom.2006.07.020

68. Song H, Cheng Y, Li B et al (2020) Carbon dots and RuP_2 nanohybrid as an efficient bifunctional catalyst for electrochemical hydrogen evolution reaction and hydrolysis of ammonia borane. ACS Sustainable Chem Eng 8:3995–4002. https://doi.org/10.1021/acssuschemeng.0c00745
69. Wu H, Cheng Y, Wang B et al (2021) Carbon dots-confined CoP-CoO nanoheterostructure with strong interfacial synergy triggered the robust hydrogen evolution from ammonia borane. J Energy Chem 57:198–205. https://doi.org/10.1016/j.jechem.2020.08.051
70. Lan X, Wang T (2020) Highly selective catalysts for the hydrogenation of unsaturated aldehydes: a review. ACS Catal 10:2764–2790. https://doi.org/10.1021/acscatal.9b04331
71. Jin J, Zhu S, Song Y et al (2016) Precisely controllable core-shell Ag@ carbon dots nanoparticles: application to in situ super-sensitive monitoring of catalytic reactions. ACS Appl Mater Interfaces 8:27956–27965. https://doi.org/10.1021/acsami.6b07807
72. Huang Q, Zhang H, Hu S et al (2014) A sensitive and reliable dopamine biosensor was developed based on the Au@ carbon dots–chitosan composite film. Biosens and Bioelectron 52:277–280. https://doi.org/10.1016/j.bios.2013.09.003
73. Toebes M (2004) Support effects in the hydrogenation of cinnamaldehyde over carbon nanofiber-supported platinum catalysts: characterization and catalysis. J Catal 226:215–225. https://doi.org/10.1016/j.jcat.2004.05.026